Studies on the Mechanical, Thermal, and Morphological Properties of Poly(ether ether ketone)/Poly(ether sulfone)/ Barium Titanate Nanocomposites: Correlation of Experimental Results with Theoretical Predictive Models

Subhash Mandal, Sarfaraz Alam

Polymer Division, Defence Materials and Stores Research and Development Establishment, G T Road, Kanpur 13, India

Received 8 July 2011; accepted 4 January 2012
DOI 10.1002/app.36735
Published online in Wiley Online Library (wileyonlinelibrary.com).

ABSTRACT: In this study, mechanical, thermal, and morphological properties of the nanocomposites fabricated with the optimized blend of poly(ether ether ketone) (PEEK) and poly(ether sulfone) (PES) incorporated with nanobarium titanate (BT) were investigated. The optimized blend was based on the mechanical and thermal properties of the PEEK and PES in the ratio of 75 : 25 wt %. Nanoparticles were incorporated into the optimized blend with the help of twin-screw extruder. The concentration of nano-BT was varied from 2 to 6 wt % (0.41–1.28 vol %). With the increase in the nanosized BT concentrations, the tensile strength, tensile modulus, and elongation at break increased, whereas the crystallinity of the nanocomposites calculated by using differential scanning calorimetry method was found to decrease marginally. Morphological studies were carried out using scanning electron microscopy. The nanocomposites were evaluated by using theoretical predictive models according to "Pukanszky model" applicable to tensile strength and "Takayanagi's model" and "Guth and Smallwood model" applicable to tensile modulus. Upper and lower boundary of Hashin–Shtrikman model as well as Paul's model, applicable to tensile modulus, were also used to compare the experimental data. © 2012 Wiley Periodicals, Inc. J Appl Polym Sci 000: 000–000, 2012

Key words: nanocomposites; mechanical properties; scanning electron microscopy (SEM); extrusion

INTRODUCTION

High performance thermoplastic polymers, blends, and composites with their many advantages are now used for various applications such as bearings, brakes and clutches, gears, office automation machinery, rollers, seals, tank track pads, transmission belts, and many others.[1–4] The combination of superior thermomechanical properties causes poly (ether ether ketone) (PEEK) as a promising candidate for applications under chemical environment at high temperatures.[5–8] Poly(ether sulfone) (PES) is an amorphous polymer with a high T_g and can be classified as a thermally stable polymer. Among other interesting properties of PES, are good hydrolytic and thermo-oxidative stability, high rigidity, and creep resistance. The high T_g of PES suggests the polymer as a suitable candidate for developing PEEK-based blends.[9,10]

Now, the interest is on high performance polymer blends based nanocomposites. Generally, polymers containing particles of the size up to 100 nm are termed as nanocomposites. Material properties of nanocomposites can substantially be different from those of respective composites with larger particles.[11,12] Due to the high surface free energy of the inorganic particles which amounts typically 500–2000 mJ/m^2, the inorganic particles in many systems, thermodynamically favor into a single sphere surrounded by the polymer.[13] Hence, the formation of nanocomposites with randomly dispersed inorganic particles is often enabled by kinetically controlled processes. Although particle agglomeration can be a problem in the fabrication of nanocomposites, the mobility of the particles is usually negligible once the nanocomposites are formed, and therefore, phase separation is suppressed in the final products even over extended periods.[11]

Recently, polymeric nanocomposites (PNCs) containing metal oxides have attracted a great deal of interest from researchers because they frequently exhibit synergistic properties.[14] Enhancement in the desired properties of PNCs has been obtained by reinforcing them with nanomaterials compared with the more conventional microparticles.[15] The control and design of characteristic structural features on the nanometer scale impart them with tailored

Correspondence to: S. Alam (sarfarazkazmi@yahoo.com).

properties for diverse applications. Development of high dielectric constant PNCs has been a major challenge of integral capacitor technology and pulse power applications.[14,16]

Inorganic fillers have been added to polymers in an attempt to increase the effective dielectric constant and energy density.[16–19] Many of the high dielectric constant PNCs was obtained at the cost of high dielectric loss and low dielectric strength.[20–22] Perhaps, the most widely investigated oxide in the field of dielectrics is barium titanate ($BaTiO_3$) (BT). The dielectric properties of BT are found to be grain size dependent and nonlinear.[23] The dielectric constant of BT (size 10 μm) is found to be in the range of 1500–2000, whereas size BT (size 1 μm) exhibits an enhanced dielectric constant[16] of 3500–6000. Nanoparticle of BT is ceramic material with high thermal stability and mechanical properties.[24]

Although our main target is to develop the high dielectric constant PNCs, in this article, we are reporting the mechanical, thermal, and morphological properties of the PEEK/PES/BT nanocomposites. Some literature is available on PEEK-based nanocomposites, but it is hardly available any literature on PEEK/PES blends based nanocomposites. Few investigation reports on PEEK-based nanocomposites are cited here as follows: Kuo et al. worked on nonisothermal crystallization kinetic behavior of alumina particle filled PEEK. They observed that the inclusion of the nanosized alumina particles can accelerate the nucleation rate due to heterogeneous nucleation but reduce the growth rate due to the retarded polymer chain mobility.[25] The resulting crystal grain size appears to be smaller in the nanocomposites. Goyal et al.[26] also studied the microhardness of PEEK/ceramic micro and nanocomposites and found that for a given volume fraction, the improvement in nanocomposites was higher than that of microcomposites. The physical and chemical properties of nanoparticles have been found to be very different from the properties of the analogous bulk materials. This specific character provides the motivation of developing materials having novel functions and properties from the existing substances.[27] The new functional nanomaterials are now one of the flourishingly attractive subjects in modern science and technology.[28] PEEK nanocomposites were fabricated by vacuum hot press molding at 400°C using nanosized SiO_2 and Al_2O_3 particulates. The resulting nanocomposites exhibit the improvement of hardness, tensile strength with the sacrifice of tensile ductility.[29–32] The aim of this work was to study the thermal and mechanical properties of PEEK/PEK/BT nanocomposites. The nanocomposites were evaluated by using theoretical predictive models according to "Pukanszky model" applicable to tensile strength and "Takayanagi's model" and "Guth and Smallwood model" applicable to tensile modulus. Upper and lower boundary of Hashin–Shtrikman model as well as Paul's model, applicable to tensile modulus, were also used to compare the experimental results.

TABLE I
Relevant Properties of PEEK, PES, and BT

Properties	PEEK	PES	BT
Bulk modulus (GPa)	3.5	2.6	67
Shear modulus (GPa)	1.3	1.1	55
Poisson ratio	0.4	0.4	0.28
Thermal conductivity (W m^{-1} K^{-1})	0.25	0.163	0.26
Density (g/cm^3)	1.303	1.370	6.01

Data collected from the literature.[9–10,24,33–35]

EXPERIMENTAL

Materials

The materials used in this study were PEEK (Victrex 450G) and PES (Trade name: RADEL, Grade: A-300) from Amoco Performance Products (Alpharetta, GA, USA) and Barium titanate ($BaTiO_3$) nanoparticles (synthesized in laboratory). PEEK is a semicrystalline polymer with glass transition temperature of 143°C and melting point of 345°C.[33,34] PES is an amorphous polymer with glass transition temperature of 223°C.[9,10] The densities of PEEK and PES are 1.303 g/cm^3 and 1.370 g/cm^3, respectively. BT nanoparticles were synthesized by reported procedure.[24] The particle size of $BaTiO_3$ was 35–80 nm. The density and melting point of $BaTiO_3$ was 6.01 g/cm^3 and 1650°C, respectively. Some relevant properties of the materials are listed in Table I.

Preparation of composites

PEEK/PES blend in the ratio of 75 : 25 by wt % was taken as the optimized blend[9,10] and designated as BS0. The optimized blend was predried at 120°C for 5 h to remove the moisture and other volatile contents. BT nanoparticles were incorporated in various concentrations viz. 2, 4, and 6 wt % (0.0041, 0.0084, and 0.0128 volume fraction (Φ_d), respectively) into the optimized blends of PEEK/PES (75/25). The nanocomposites of PEEK/PES/BT were compounded in Prism Eurolab-16 twin-screw extruder. The molten extrudate was quickly quenched in a water bath to room temperature. The compound thus obtained were collected as strands and cut into granules using automatic chopper. The chopped granules were predried at 120°C for 10 h and molded by injection molding for further characterization. The optimized blends (BS0) reinforced by 0.41, 0.84, and 1.28 vol % of BT nanoparticles are designated as BS1, BS2, and BS3, respectively. The

TABLE II
Composition Details of the Nanocomposites

Sample	Filler content (vol %)
BS0	0
BS1	0.41
BS2	0.84
BS3	1.28

composition details of the nanocomposites are given in Table II.

Characterization

The thermal behavior of the PEEK/PES/BT nanocomposites was evaluated using Universal TA instrument [differential scanning calorimeter (DSC) V4.5A, TA Instruments, USA]. The weight of all samples were 5–7 mg, and these samples were heated to 400°C at constant heating rate of 10°C/min under nitrogen atmosphere to study the melting behavior, and held for 5 min to remove the previous thermal history. Nonisothermal crystallization was investigated by cooling the samples from 400°C to 50°C at constant cooling rate of 10°C/min. The thermal behavior was also carried out using Modulated DSC (MDSC) mode at a heating rate of 2°C/min with the temperature modulation amplitude of ±1.0–1.5°C for the modulation period of 60 s to verify the DSC results, especially T_g.

Tensile properties were determined by a universal testing machine (Zwick 1773, ZWICK, Germany) at room temperature. The injection molded samples of standard tensile (ASTM D638) bar. The cross-head separation was 6 cm, and cross-head speed was 5 mm/min during the tensile test following the ASTM D638 test method.[36] A minimum of five samples were tested for each composition and their average value within ±3.5% is reported. The test were performed at ambient temperature 303 ± 2 K. Compounded materials were used in a scanning electron microscope (SEM; EVO-50, CARL ZEISS, Germany) to study the morphology of the blend and nanocomposites samples. The acceleration voltage used was 10 kV, and the magnification was 1000× for sample BS0 and 9000× for samples BS1, BS2, and BS3. The samples were coated with a thin layer of gold by using a vacuum sputtered before SEM observations.

Theoretical predictive model used

To understand the role of BT nanoparticles in the nanocomposites structure, the data were analyzed according to the following theoretical predictive models.

Models related to tensile modulus

Model 1: Guth and Smallwood Model[37,38]

For spherical particles

$$E_c/E_m = 1 + K_E\Phi_d + 14.1\ \Phi_d^2 \quad (1)$$

For nonspherical particles

$$E_c/E_m = 1 + 0.67\alpha\Phi_d + 1.62\ \alpha^2\Phi_d^2 \quad (2)$$

where E, tensile modulus; Φ, volume fraction; c, m, and d indicates composite, matrix, and dispersive phase, respectively; K_E, Einstein coefficient[39] = 2.5 for spherical particles; α, reinforcement aspect ratio (AR)[40] = 1.0–1.3.

Model 2: Takayanagi's model[41]

A three-phase model, proposed by Ji et al.,[42] taking into account the matrix, the filler particles and the interphase. For plate particles having thickness t_c and both length and width ξ_c (with $\xi_c \gg t_c$), tensile modulus can be expressed as of the following equation:

$$\frac{E_c}{E_m} = \left((1-\alpha) + \frac{\alpha-\beta}{(1-\alpha)+\alpha(k-1)/\ln(k)} + \frac{\beta}{(1-\alpha)+(\alpha-\beta)(k+1)/2+(E_f/E_m)\beta}\right)^{-1} \quad (3)$$

where $\beta = \sqrt{(\Phi_d)}$; $\alpha = \sqrt{[\{2(\tau/t_c)+1\}\Phi_d]}$; E_c, E_m, and E_f are tensile modulus of the composite, matrix, and the filler, respectively; τ is the thickness of the interphase; Φ_d is the filler volume fraction; and $k = E_i(0)/E_m$ is the ratio of the interphase modulus on the surface of the particle, $E_i(0)$, to that of the matrix, E_m. This three-phase model assumes linear dependence of the modulus on space variable, when passing from the matrix to the surface of the particle. The controlling parameters for the mechanical properties of the materials are the two characteristic dimensions of the dispersed particles, t_c and ξ_c, the thickness of the interphase, τ, the ratio E_f/E_m and the parameter k. If the influence of the interfacial region can be neglected, corresponding to $\tau = 0$ (means $\alpha = \beta$), then the three-phase model reduces to the two-phase Takayanagi's model[41] eq. (4).

$$\frac{E_c}{E_m} = \left((1-\beta) + \frac{\beta}{(1-\beta)+(E_f/E_m)\beta}\right)^{-1} \quad (4)$$

According to Ji et al.,[42] the smaller particles provide an increasing modulus for the resulting composite when compared with the large particles because the interfacial region greatly affects E_c. However, when the size of the fillers is in the scale of micrometers, the influence of the interfacial region is neglected. In this case, as nanoparticles were used, thickness of the interfacial region can be assumed to tend to zero.

Model 3: Hashin–Shtrikman model[43]

The two-phase model related to tensile modulus proposed by Hashin and Shtrikman[43] who took into account the Poisson contraction of the constituent phases. The overall response of the composite was assumed to be isotropic and linearly elastic. The equations for the lower and upper bounds are given in eqs. (5) and (6), respectively.

$$E_c = \frac{9\left(K_d + \frac{\Phi_m}{[1/(K_m - K_d)] + [3\Phi_d/(3K_d + 4G_d)]}\right)\left(G_d + \frac{\Phi_m}{[1/(G_m - G_d)] + [6(K_d + G_d)\Phi_d/5(3K_d + 4G_d)G_d]}\right)}{3\left(K_d + \frac{\Phi_m}{[1/(K_m - K_d)] + [3\Phi_d/(3K_d + 4G_d)]}\right) + \left(G_d + \frac{\Phi_m}{[1/(G_m - G_d)] + [6(K_d + G_d)\Phi_d/5(3K_d + 4G_d)G_d]}\right)} \quad (5)$$

$$E_c = \frac{9\left(K_m + \frac{\Phi_d}{[1/(K_d - K_m)] + [3\Phi_m/(3K_m +}\right)\left(G_m + \frac{\Phi_d}{[1/(G_d - G_m)] + [6(K_m + G_m)\Phi_m/5(3K_m + 4G_m)}\right)}{3\left(K_m + \frac{\Phi_d}{[1/(K_d - K_m)] + [3\Phi_m/(3K_m +}\right) + \left(G_m + \frac{\Phi_d}{[1/(G_d - G_m)] + [6(K_m + G_m)\Phi_m/5(3K_m + 4G_m)G_m]}\right)} \quad (6)$$

where K and G are the bulk and shear moduli and m and d refers to matrix and dispersed phase, respectively.

Model 4: The Paul's model

The model proposed by Paul[44] for the approximate solution of the tensile modulus, the constituents are assumed to be in a state of macroscopically homogeneous stress. Adhesion is assumed to be maintained at the interface of a cubic inclusion embedded in a cubic matrix. When a uniform stress is applied at the boundary the elastic modulus of the composite is given by

$$\frac{E_c}{E_m} = \frac{1 + (m-1)\Phi_d^{2/3}}{1 + (m-1)(\Phi_d^{2/3} - \Phi_d)} \quad (7)$$

Models related to tensile strength

Pukanszky model[45–47]

$$\frac{\sigma_c}{\sigma_m} = \frac{1 - \Phi_d}{1 + 2.5\ \Phi_d}\ \exp(B_\sigma \Phi_d) \quad (8)$$

where the fraction $[(1 - \Phi_d)/(1 + 2.5\ \Phi_d)]$ takes into consideration the decrease of the effective load bearing cross-section,[48] and the exponential describes all other effects resulting in an increase of the tensile strength. σ_c and σ_m is the tensile strength of composites and matrix, respectively.

From the physical point of view, the parameter B_σ is governed by the interface and interphase properties. Indeed, as shown by Rong et al.[49] for polypropylene nanocomposites, larger B_σ values correspond to higher interfacial adhesion. The following B_σ expression underlines these effects:

$$B_\sigma = (1 + \tau\rho_f S_f)\ \ln\ \frac{\sigma_i}{\sigma_m} \quad (9)$$

where t, the thickness of the interphase, is proportional to the interfacial adhesion, defined by the parameter γ_{12}, with $\tau = \lambda\gamma_{12}$, where λ is constant. The quantities ρ_f, S_f, and σ_i represent the density of the filler material, the specific surface area of the filler, and the yield stress of the interphase, respectively.

Because it is virtually impossible to provide exact values for the absolute thickness t and for the yield stress σ_i of the interphase, the parameter B_σ was determined from the experimental data using the following expression, derived from eq. (8):

$$B_\sigma = \frac{1}{\phi_d}\ \ln\left(\frac{\sigma_c}{\sigma_m}\ \frac{1 + 2.5\ \Phi_d}{1 - \Phi_d}\right) \quad (10)$$

RESULTS AND DISCUSSION

DSC analysis

The thermal behavior of the PEEK/PES/BT nanocomposites were studied by DSC and shown in Figures 1 and 2. As shown in Figure 1, there is no significant change in the melting points, T_m, of both the filled and unfilled samples in the DSC diagram.

The melting temperatures are 343.5 ± 1.5°C, in the typical range of 342–345°C. There are several factors involved due to the addition of nanoparticles on the crystallization; some of them are counteracting each other making the neat effect obscure sometimes. For example, in terms of heterogeneous nucleation of PEEK/PES on the nanoparticles interfaces, the crystallization and peak temperature might increase. However, the obstacle effect from the nanoparticles on PEEK and PES chain mobility would lower the crystallization temperature.[32] Table III summarizes the data on glass transition temperature (T_g), melting temperature (T_m), initial crystallization temperature (T_{ci}), peak crystallization temperature (T_{cp}), final crystallization temperature (T_{cf}), and the fusion enthalpy, H_f, for the neat blend and nanocomposites. From the results, it can be observed that the T_g increased (Fig. 2) marginally due to the dispersion

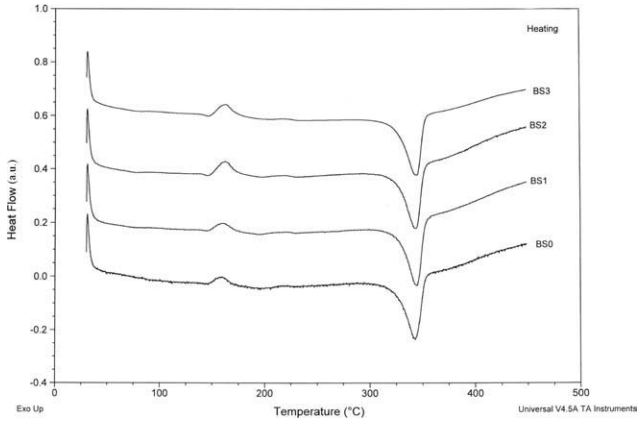

Figure 1 DSC heating curves of PEEK/PES/BT nanocomposites at a heating rate of 10°C/min.

of nanoparticles, heterogeneous nucleation and close packing of the materials. The improvement in tensile modulus might be attributed to the good adhesion between the matrix and the nanoparticles, which restrict the segmental motion of the matrix.[39] As a result, marginal increase of T_g was observed. The T_g obtained from the DSC results were verified using MDSC mode and the obtained results were almost the same (not shown). The result of marginal increase of T_g can also be explained by the change in thermal conductivity by adding BT. At lower BT concentration with uniform nanoparticles dispersion, the nanocomposites usually have the higher volume of interfaces. Due to the presence of these interfaces, thermal conductivity of the composite becomes relatively low. As a result, the T_g increased slightly; but at higher concentration of BT, thermal conductivity does not decrease further when the interfaces are overlapping and will be reduced due to the agglomeration of nanoparticles. Therefore, T_g does not increase after certain concentration of BT nanoparticles in the nanocomposites.

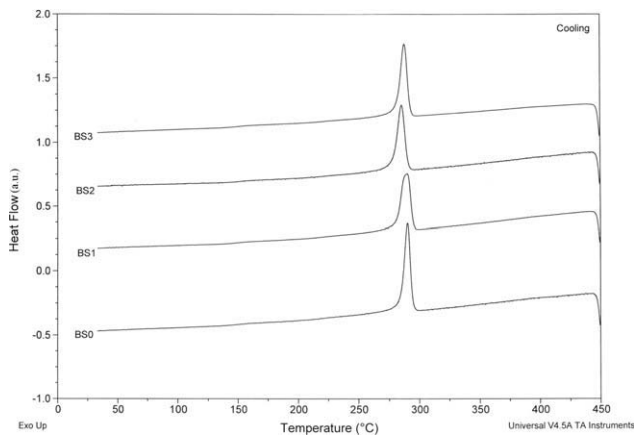

Figure 2 DSC cooling curves of PEEK/PES/BT nanocomposites at a cooling rate of 10°C/min.

From the DSC diagrams, the absolute crystallinity fraction (X_c) was estimated by relating the heat of fusion of an infinitely thick PEEK crystal, ΔH_f^0, from the following equation[40]:

$$X_c = \Delta H_f x100/\ \Delta H_f^0 x W_{\text{polymer}} \tag{11}$$

where ΔH_f^0 is approx. 130 J g^{-1}, and W_{polymer} is the weight fraction of polymer matrix.[50]

The crystallinity of PEEK/PES/BT nanocomposites decreased marginally in comparison with the crystallinity of neat blend. The decrease of crystallinity was due to the disturbance of the polymer chain alignment in presence of nanoparticles and accounting for the lower mobility of the PEEK and PES chain segments at high nanoparticles content[32]; but the same was found to increase in the presence of increasing contents of the nanoparticles of BT. This happened due to the heterogeneous nucleation on the surface of nanoparticles and due to the phase segregation. Therefore, the overall effect on crystallinity gradually decreased and hence the crystallinity value of nanocomposites is very close to that of neat blend. By closer examination of the DSC curves, it was found that the crystallization temperature and crystallinity fraction X_c of the filled matrix were affected slightly by the amount of nanoparticles, whereas the melting temperature T_m remaining unchanged.

Tensile properties

The tensile properties were first determined from the primary stress–strain curves of the blends and nanocomposites (not shown). In Figures 3–7, the results are presented as the ratio of the property of the nanocomposites (subscript c) to that of the PEEK/PES blend as matrix (subscript m) vs. Φ_d of the BT nanoparticles.

Tensile modulus

Figure 3 shows the plot of relative tensile modulus, E_c/E_m, of the PEEK/PES/BT nanocomposites against Φ_d. The modulus increased with increase in Φ_d, at

TABLE III
DSC Data of the PEEK/PES/BT Nanocomposites

Sample	T_g (°C)	T_{ci} (°C)	T_{cp} (°C)	T_{cf} (°C)	T_m (°C)	H_f (J g^{-1})	X_c (%)[a]
Neat PEEK	145.78	313	302	283	340.31	−43.81	33.70
BS0	159.46	295	289	274	342.76	−24.54	25.17
BS1	160.44	294	288	271	344.94	−23.06	24.13
BS2	162.43	291	285	270	343.59	−23.16	24.74
BS3	162.89	293	287	268	344.64	−22.92	25.01
BT	–	–	–	–	1650	–	–

[a] The error in estimating X_c is 0.01% (instrumental).

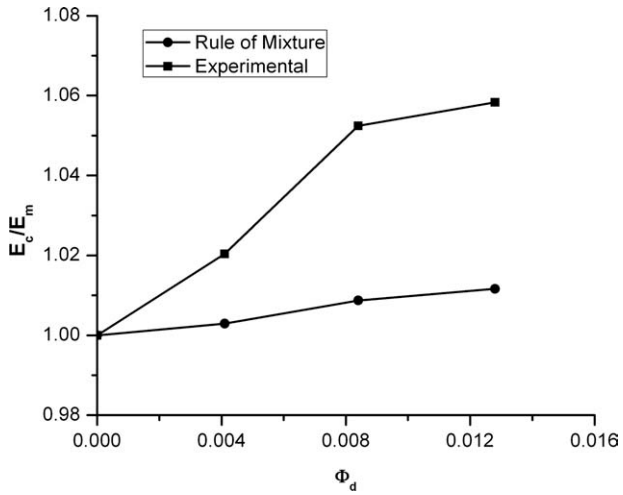

Figure 3 Plot of relative tensile modulus, E_c/E_m, of PEEK/PES/BT nanocomposites with experimental (■) and the "rule of mixtures" (●), against Φ_d.

the highest Φ_d (1.28 vol %) the modulus increased by approx. 5.8% from that of the matrix. Whereas the increase in modulus at Φ_d (0.84 vol %) was 5.2%. This indicates that PEEK/PES blend is stiffened to an extent by the nanoparticles of BT.

To understand the role of BT nanoparticles in the nanocomposites structure the data were analyzed according to simple predictive model following the "rule of mixture"[51,52] as in composites and blends, eq. (12),

$$E_m = \Phi_1 E_1 + \Phi_2 E_2 \tag{12}$$

In the above equation, E_m, E_1, and E_2 are the modulus of the blends, PEEK, and PES, respectively. Φ_1 and Φ_2 are the volume fraction of PEEK and PES, respectively.

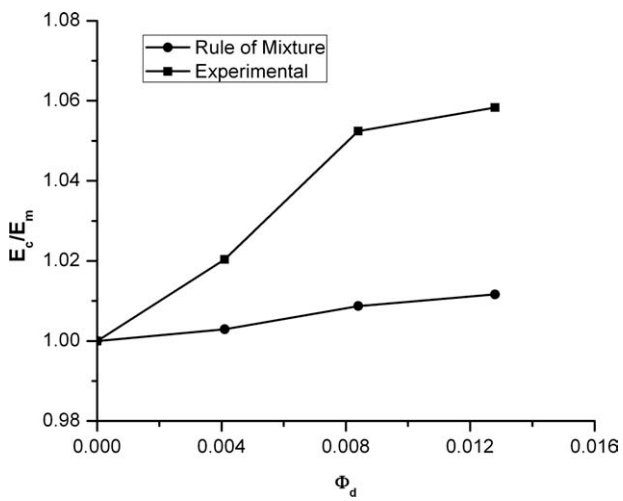

Figure 4 Comparison of relative tensile modulus, E_c/E_m, of PEEK/PES/BT nanocomposites results obtained from experimental (■), Guth model [with AR (aspect ratio) = 1.0 (▼), AR = 1.2 (●), and AR = 1.3 (▲)], and Takayanagi's model (◀) against Φ_d.

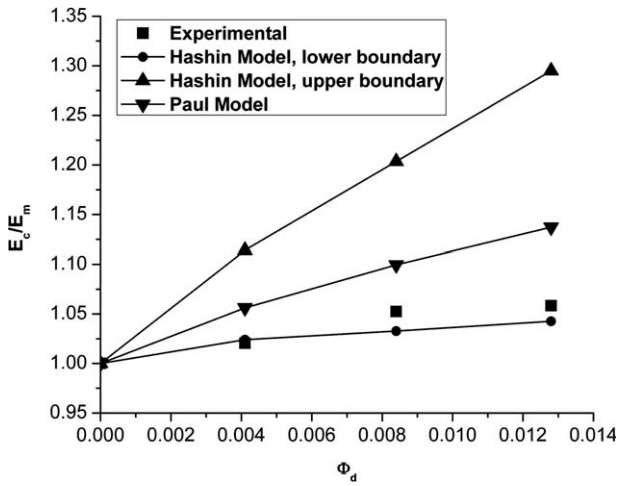

Figure 5 Variation of relative tensile modulus, E_c/E_m, of PEEK/PES/BT nanocomposites results obtained from experimental (■), Hashin–Sthrikman's model [upper boundary (▲) and lower boundary (●)], and the Paul's model (▼) against Φ_d.

Because there is no widely accepted addition rule for the nanocomposites modulus (or strength), it is simply evaluated (for BS1, BS2, and BS3) by the "modified rule of mixture for discontinuous reinforcement"[1,32] eq. (13).

$$E_c = \eta E_d \Phi_d + E_m \Phi_m \tag{13}$$

where E is the tensile modulus, Φ is the volume fraction, and the subscripts c, d, and m represent the composite, particle, and matrix (PEEK/PES blend), respectively. The strengthening efficiency coefficient η would decrease rapidly with decreasing reinforcement AR.[1] Extending the values for short fibers with ARs of 10–100 to the range for nanoparticles with an

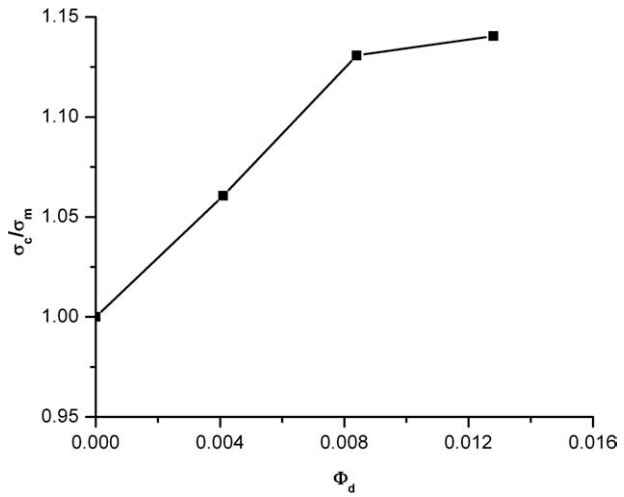

Figure 6 Plot of relative tensile strength, σ_c/σ_m, of PEEK/PES/BT nanocomposites (■).

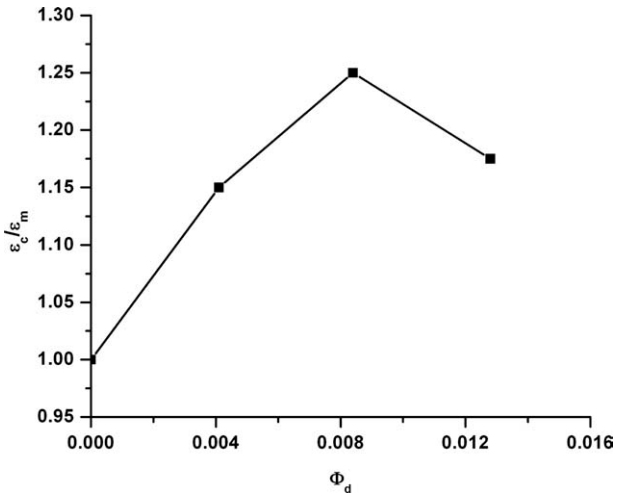

Figure 7 Variation of relative elongation-at-break, $\varepsilon_c/\varepsilon_m$, of PEEK/PES/BT nanocomposites (■) against Φ_d.

AR of around 1, η is assumed to be approx. 0.1.[32] The "rule of mixture" exhibited lower value of the relative modulus of the nanocomposites than the experimental data. This deviation was found because in the "modified rule of mixture for discontinuous reinforcement" in eq. (13) assumed values [e.g., η in eq. (13)] were used. This indicates that the dispersed phase increases the stiffness of the PEEK/PES blends. The "modified rule of mixture for discontinuous reinforcement" does not have any parameters related to interfacial adhesion as well as crystallinity due to heterogeneous nucleation. In consequence of this, the nanocomposites in which heterogeneous nucleation takes place and interfacial adhesion varies, such a deviation between "rule of mixture" and "experimental results" is observed.

Equations (1)–(7) were used to fit the tensile modulus experimental values reported in the article. The filler tensile modulus is $E_f = 67$ GPa, and the measured Young Modulus of the matrix was $E_m = 3.43$ GPa, corresponding to $E_f/E_m = 19.53$. All the results obtained from the predictive models and the relative tensile moduli of the nanocomposites are shown in Figure 4. It is seen that the "Guth and Smallwood model" deviate significantly from the experimental results for all AR, i.e., AR = 1.0, AR = 1.2, and AR = 1.3. The Takayanagi's model is closely fitted up to $\Phi_d = 0.84$ vol %. The decrease in relative tensile modulus was due to the weaker interfacial adhesion at $\Phi_d = 1.28$ vol %. Regarding "Paul model" no correlation to the experimental results could be found. However, the lower boundary of the Hashin–Shtrikman model (shown in Fig. 5) shows good correlation with experimental results.

The different models used for the prediction of the moduli of a filled system, their limitations will be discussed here. In the above discussion, no attempt has been made to discuss the approaches in detail but to demonstrate the different theoretical hypotheses to describe the moduli of the filled system. For a discussion of the detailed theoretical base of each the reader is referred to Hashin[53] and Hill.[54] The lower and upper bound solutions given by eqs. (5) and (6) assume that the individual phases are under uniform strain or stress, respectively, However, in practical case, the filler particles may not be completely separated from one another and the reinforcement element may effectively be an aggregate of smaller particles. Therefore, in response to the applied load, the stress will be distributed unevenly between the particles and aggregates and the assumptions of either uniform strain is clearly an oversimplification.

To account for the complex stress and phase distribution, different models considered different combinations of the upper and lower bounds of the laws of mixtures. An empirical factor which is determined by a curve fitting routine is required for all of these models to furnish a phenomenological description of the experimental data.

Tensile strength

Figure 6 shows the plots of relative tensile strength, i.e., ratio of tensile strength of nanocomposites to that of PEEK/PES blend, σ_c/σ_m, vs. Φ_d. The tensile strength showed a continuous increase with increasing Φ_d indicating that the nanocomposite structure was strengthened by the nanoparticles. At $\Phi_d = 1.28$ vol %, the tensile strength of the nanocomposites was found to increase by 14% to that of the matrix, whereas the same was found to increase by around 13% at $\Phi_d = 0.84$ vol %.

The predictive model proposed by Pukanszky et al.[45–47] was used to study the tensile strength data of the nanocomposites to assess the level of interfacial interaction. The model was selected to study the ratio of the tensile strength of the nanocomposites to that of the neat blend PEEK/PES as matrix as a function of the filler volume fraction Φ_d.

The values of B_σ are listed in Table IV. The table shows that B_σ increases up to $\Phi_d = 0.84$ vol % and then decreases sharply for higher volume fraction. This result could be explained by the fact that, up to 0.84 vol %, adding fillers tends to improve, on

TABLE IV
Value of B_σ Parameter Obtained From Pukanszky MODEL

Sample	B_σ value
BS0	–
BS1	17.73
BS2	18.11
BS3	13.73

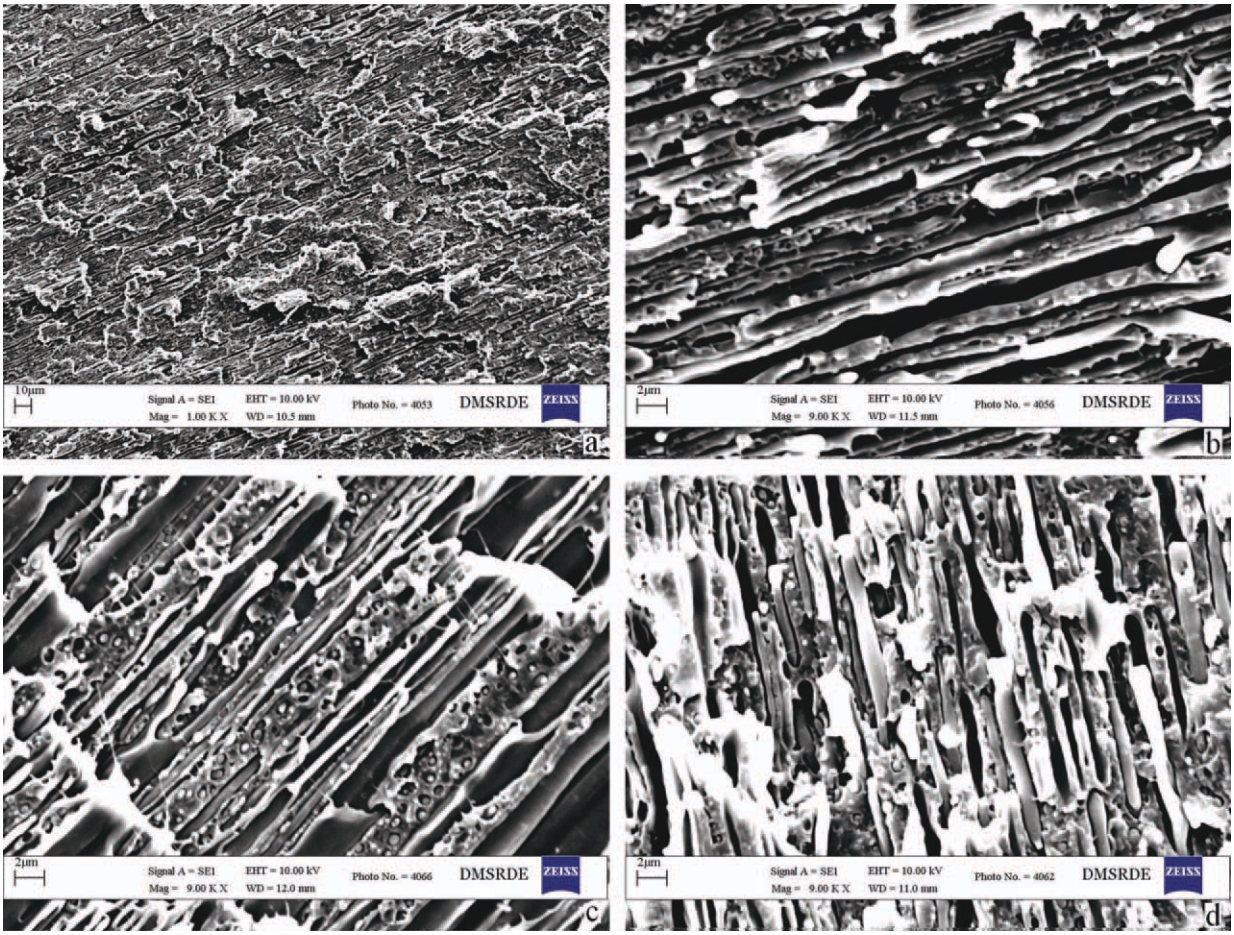

Figure 8 SEM photographs of PEEK/PES/BT nanocomposites at various filler content (vol %): (a) 0; (b) 0.41; (c) 0.84, and (d) 1.28. [Color figure can be viewed in the online issue, which is available at wileyonlinelibrary.com.]

average, interfacial PEEK/PES/BT adhesion. However, at higher volume fraction, the agglomeration of the nanoparticles increases (shown in phase morphology section), leading to a significant decrease in the average specific surface area of the BT nanoparticles, which is highlighted herein by the sharp decrease of the B_σ parameter.

Particle size can greatly affect the tensile strength of the different filled system. The tensile strength increases with a decrease in particle size. The increase in interfacial area which provides a more effective interfacial bond is considered to be the most important factor. Particle size is also related to the flaw size dependence of the material. Goodier[55] has shown that the stress field near a particle is independent of particle size. However, the volume of polymer that experiences a given stress concentration is increased with increase in particle size. Therefore, the probability of finding large flaw increases with increased particle size.

The effect of interfacial adhesion on the strength can be rationalized in a similar fashion because a poor particle–matrix bond will act as an inherent flaw with the production of a cavity equal to its size. The shape of the inclusion is expected to play an important role in determining the strength of the filled system. Because, with a nonregularly shaped inclusion, the weakening is due to a high stress concentration coupled with a size effect, and with rounded cracks and inclusions the stress is much less severe than for inclusions with sharp corners.

Elongation at break

Variations of relative strain-at-break, $\varepsilon_c/\varepsilon_m$, vs. Φ_d are shown in Figure 7. It was found that the elongation at break of the nanocomposites is higher than that of the neat matrix. The value increases with increase in Φ_d up to $\Phi_d = 0.84$ vol % and then the value decreased. As evidenced by the white bands appearing during the test at the centre of the samples, large-scale plastic deformations occurred perpendicular to the tensile direction. The whitening intensified and the bands coalesced before fracture occurred across one of them when the mechanical loading increased. These types of bands were not observed for neat blends. The existence of such bands could be attributed to the presence of agglomerates,

as suggested by Thio et al.[56] for polypropylene filled with $CaCO_3$.

The capacity to withstand large deformations of the nanocomposites comes with the possible microvoid formation and with probable detachment of polymer matrix and nanoparticles when loading the sample.[57] The microvoid forms at the interface due to the irregular shape of the dispersed particles and during heterogeneous nucleation due to the formation crystal lattice of different size and shape. For $\Phi_d = 1.28$ vol %, the voids become so numerous, so large and sufficiently close together that they coalesce, causing a catastrophic macroscopic fracture of the material at weak strains and stresses.[58] The same can also be explained by the percolation theory.[42,48]

Based on the percolation concept, both interfacial region and a dispersed particle as a percolation cluster were considered. The percolation clusters are disconnected and well separated from one another at low volume fraction of the dispersed phase. The volume of interfacial layers increases resulting interaction of the percolation clusters at higher volume fraction of the dispersed phase. In the case of agglomeration, this interfacial layers overlap with each other. As a result, fracture of the material occurs at weak strains and stresses.

Phase morphology

The phase morphology of the optimized blend and nanocomposites was carried out on the samples obtained after compounding using SEM. It is well known that the nanoparticles form agglomerate in the polymer matrix, and in turn decrease the reinforcing effect. The nanoparticles are difficult to be well resolved by the secondary or back scattering electron images under SEM, because the contrast is generally weak.[59] The SEM photomicrographs of PEEK/PES/BT nanocomposites at varying Φ_d are shown in Figure 8(a–d).

It is seen that the dispersion condition of the nanoparticles in the matrix are reasonably uniform in the BS1 and BS2 nanocomposites. Segregation of nanoparticles is observed in all the nanocomposites. The nanoparticles sizes in the SEM photographs are higher than mentioned in the materials section. It was found because nanoparticles of BT are highly agglomerated to form large (100–300 nm), irregular shaped aggregates.[60] However, the agglomeration degree increases with increasing nanoparticles content. It happened because the increased viscosity of the matrix and nanoparticles mixture at higher nanoparticles contents during the processing. Besides the increased viscosity of the matrix and nanoparticles mixture, the relatively low shear force while processing and sterically "bonding" of the nanoparticles could be a reason for agglomeration.

CONCLUSIONS

The observed PEEK/PES/BT nanocomposites have shown enhancement of the tensile strength, tensile modulus and elongation at break with volume fraction of BT up to $\Phi_d = 0.84$ vol %, meaning a significant improvement in mechanical properties. At volume fraction higher than 0.84 vol %, tensile modulus of the nanocomposites was found to increase, but very small extent, whereas the other mechanical properties reported in this article were found to decrease with increasing nanoparticles content. The enhancement of the tensile strength and modulus was due to the significant interfacial adhesion in the nanocomposites.

Thermal properties exhibited marginal increase of T_g with the increase of nanoparticles content.

Phase morphology shows the segregation of the nanoparticles for all examined nanocomposites, however at higher Φ_d agglomeration was observed.

Theoretical predictive model, e.g., "Takayanagi's model" applicable to tensile modulus showed very close correlation to experimental results up to $\Phi_d = 0.84$ vol %. However, the lower boundary of the Hashin–Shtrikman model is the most suitable one compared with experimental results. It was shown from the "Pukanszky model," applicable to tensile strength, that the tensile strength of the nanocomposites seemed to be governed by the parameter B_σ, which relates interface and interphase interaction.

The authors thank to the Director, DMSRDE, Defence Research and Development Organization for giving permission to publish the articles. The authors would also like to acknowledge the help of Mr. Ram Prakash, Mr. Hari Babu Gupta, and Ms. Kavita Agarwal.

References

1. Hull D. An Introduction to Composite Materials; Cambridge University Press: Cambridge, 1981.
2. Paul D. R.; Newman S., Eds. Polymer Blends; Academic Press: New York, 1978;Vols.1/2.
3. Utracki L. A. Polymer Alloys and Blends-Thermodynamics and Rheology; Hanser Publishers: Munich, 1989.
4. Olabisi O.; Robeson L. M.; Shaw M. T. Polymer–Polymer Miscibility; Academic Press: New York, 1979.
5. Zachariades A. E.; Porter R. S., Eds. High Modulus Polymers; Marcel Dekker: New York, 1988.
6. Hegazy EI-S. A.; Sasuga T.; Nishii M.; Seguchi T. Polymer 1992, 33, 2897.
7. Thompson S. A.; Farris R. J. J Appl Polym Sci 1988, 36, 1113.
8. Nishino T.; Tada K.; Nakamae K. Polymer 1992, 33, 736.
9. Nandan B.; Kandpal L. D.; Mathur G. N. Eur Polym J 2003, 39, 193.
10. Nandan B.; Kandpal L. D.; Mathur G. N. J Appl Polym Sci 2003, 90, 2887.
11. Caseri W. In The Chemistry of Nanostructured Materials; Yang P., Ed.; World Scientific Publishing Co. Pte. Ltd.: USA, 2003.
12. Bose S.; Mahanwar P. A. J Mater Sci 2005, 40, 6423.

13. Kinloch A. J. Adhesion and Adhesives; Chapman and Hall: London, 1987.
14. Mallikarjuna N. N.; Manohar S. K.; Kulkarni P. V.; Venkataraman A.; Aminabhavi T. M. J Appl Polym Sci 2005, 97, 1868.
15. Novak B. M. Adv Mater 1993, 5, 422.
16. Barber P.; Balasubramanian S.; Anguchamy Y.; Gong S.; Wibowo A.; Gao H.; Ploehn H J.; Loye H. C. Z. Materials 2009, 2, 1697.
17. Rao Y.; Yue J.; Wong C. P. Active Passive Elect Comp 2002, 25, 123.
18. Joo J.; Long S. M.; Pouget J. P.; Oh E. J.; MacDiarmid A. G.; Epstein A. J. J Phys Rev B 1998, 57, 9567.
19. Tuncer E.; Rondinone A. J.; Woodward J.; Sauers I.; James D. R.; Ellis A. R. Appl Phys A 2009, 94, 843.
20. Dang Z. M. Adv Mater 2003, 15, 1625.
21. Pecharroman C.; Esteban-Betegon F.; Bartolome J. F.; Lopes-Esteban S.; Moya J. S. Adv Mater 2001, 13, 1541.
22. Qi L. Adv Mater 2005, 17, 1777.
23. Robertson J.; Hall D. A. J Phys D: Appl Phys 2008, 41, 115407.
24. Phule P. P.; Risbud S. H. Adv Ceram Mater 1988, 3, 183.
25. Kuo M. C.; Huang J. C.; Chen M. Mater Chem Phys 2006, 2–3, 258.
26. Goyal R. K.; Tiwari A. N.; Negi Y. S. Mater Sci Eng A 2008, 491, 230.
27. Day M.; Suprunchuk T.; Cooney J. D.; Wiles D. M. J Appl Polym Sci 1988, 36, 1097.
28. Liu Y. L.; Li S. H. J Appl Polym Sci 2005, 95, 1237.
29. Nandan B.; Kandpal L. D.; Mathur G. N. Polymer 2003, 44, 1267.
30. Goyal R. K.; Tiwari A. N.; Mulik U. P.; Negi Y. S. Compos Sci Technol 2007, 67, 1802.
31. Blundell D. J.; Osborn B. N. Polymer 1983, 24, 953.
32. Kuo M. C.; Tsai C. M.; Huang J. C.; Chen M. Mater Chem Phys 2005, 90, 185.
33. Nandan B.; Lal B.; Pandey K. N.; Alam S.; Kandpal L. D.; Mathur G. N. Eur Polym J 2001, 37, 2147.
34. Mandal S.; Alam S. J Appl Polym Sci 2010, 117, 849.
35. Hosokawa M.; Nogi K.; Naito M.; Yokoyama T. Nanoparticle Technology Handbook; Elsevier: Amsterdam, 2007.
36. Annual book of ASTM standard, Philadelphia, Part 37, 1976.
37. Guth E. J Appl Phys 1945, 16, 20.
38. Ahmed S.; Jones F. R. J Mater Sci 1990, 25, 4933.
39. Goyal R. K.; Tiwari A. N.; Negi Y. S. J Appl Polym Sci 2011. doi:10.1002/app.33684.
40. Som T.; Karmakar B. J Opt Soc Am B 2009, 26, B21.
41. Takayanagi M.; Uemura S.; Minami S. J Polym Sci Part C 1964, 5, 113.
42. Ji X. L.; Jing J. K.; Jiang W.; Jiang B. Z. Polym Eng Sci 2002, 42, 983.
43. Hashin Z.; Shtrikman S. J Mech Phys Solid 1963, 11, 127.
44. Paul B. Trans Am Inst Mech Eng 1960,36, 218.
45. Pukanzsky B.; Fekete E. Adv Polym Sci 1999, 139, 109.
46. Pukanzsky B.; Turcsanyi B.; Tudos F.; Ishida H., Eds. Interfaces in Polymer, Ceramics and Metal Matrix Composites; Elsevier: New York, 1988, p 467.
47. Pukanzsky B.; Voros G. Compos Int 1993, 1, 411.
48. Nicolais L.; Narkis M. Polym Eng Sci 1971, 11, 194.
49. Rong M. Z.; Zhang M. Q.; Pan S. L.; Lehmann B.; Friedrich K. Polym Int 2004, 53, 176.
50. Wei C. L.; Chen M.; Yu F. E. Polymer 2003, 44, 8185.
51. Agarwal B. D.; Broutman L. J. Analysis and performance of fiber composites; Wiley and Sons: New York, 1990; Chapter 3.
52. Maiti S. N.; Das R. Int J Polym Mater 2005, 54, 467.
53. Hashin Z. Appl Mech Rev 1964, 17, 1.
54. Hill R. J Mech Phys Solid 1963, 11, 357.
55. Goodier J. N. J Appl Mech Trans 1933, AME A3, 55.
56. Thio Y. S.; Argon A. S.; Cohen R. E.; Weinberg M. Polymer 2002, 43, 3661.
57. McNally T.; Murphy W. R.; Lew C. Y.; Turner R. J.; Brennan. P. Polymer 2003, 44, 2761.
58. Hocine N. A.; Mederic P.; Aubry T. Polym Testing 2008, 27, 330.
59. Sandler J.; Werner P.; Shaffer M. S. P.; Demchuk V.; Altstadt V.; Windle A. H. Composites A 2002, 33, 1033.
60. Nicodemo L.; Nicolas L. Mater Sci Lett 1983, 2, 201.